CrossMark

Synthesis and characterization of organic nonlinear optical material: urea *para*-nitrophenol

S. Selvakumar[1] · A. Leo Rajesh[1]

Abstract The organic nonlinear single crystals of urea *para*-nitrophenol (UPN) have been grown using slow evaporation solution growth technique. The formation of the organic product has been confirmed by CHN analysis. The structure of grown crystal was examined by single-crystal X-ray diffraction technique. The presences of functional groups were identified from FT-IR spectrum. The large transmittance properties of the crystal and its linear band gap energy of 3.18 eV inform that the material is suitable for optoelectronic applications. The TG–DTA curve confirms that the grown crystal was thermally stable up to 120 °C. Dielectric constant and dielectric loss values were also measured as a function of frequency between 5 Hz and 5 MHz and temperature from 40 to 100 °C. The second-harmonic generation efficiency of the UPN crystal is found to be 3.5 times greater than that of KDP crystal. The NLO parameters intensity dependent refractive index (n_2), non-linear absorption coefficient (β) and third-order susceptibility $|\chi^3|$ were calculated using Z-scan techniques. The morphology of its UPN crystal was studied using SEM analysis.

1 Introduction

The organic crystals are having versatile applications in frequency doubling, frequency mixing, electro optic modulation, optical storage and optical communications [1]. In the organic compounds, presence of electron rich (donor) and deficient (acceptor) substituents provide the infrastructure to induce asymmetric charge distribution in the π electron system and hence large nonlinear optical responses [2]. Nonlinear optical (NLO) crystals should possess several requirements, like large phase-matchable nonlinear optical co-efficient, high damage threshold, wide optical nonlinearity and chemical stability to be considered as NLO material [3, 4]. In general, the organic crystals are found to have high nonlinear optical efficiencies and additionally offer large number of design possibilities. Optical nonlinearity of the organic molecules can be altered by addition of suitable electron donating/withdrawing entities. This is mainly due to the asymmetric molecules carry a dipole moment in their ground electronic state, and in order to reduce the dipole–dipole interaction, which is dominant over the van der Waals interaction in the lattice [5].

Among the organic crystals, urea and its derivatives explored extensively, due to their coherent NLO properties [6, 7]. However urea has some undesirable properties, such as mechanically soft and hygroscopic nature. Hence, the urea cannot be used in normal atmosphere [8]. Hence it is used by immersing it in an index-matching fluid with compatible chemical and optical characteristics. During the past decade, researchers have shown much attention in *para*-nitrophenol family of crystals due to their high laser damage threshold, transparency window, extended thermal stability and high NLO co-efficient [9, 10]. *Para*-nitrophenol totally matches this criterion with its electron donor substituents "–OH" and electron acceptor substituents "–NO_2" and phenyl group form a conjugated molecular configuration [11, 12]. *Para*-nitrophenol derivatives are interesting candidates as they are a typical one dimensional donor–acceptor π system, and the presence of phenolic OH favors the formations of salts with various organic and inorganic bases [13]. Generally, the bulk materials are used in frequency conversion, frequency doubling, laser technology etc., whereas the nano particles are

✉ A. Leo Rajesh
aleorajesh@gmail.com

1 Department of Physics, St. Joseph's College (Autonomous), Tiruchirappalli, Tamil Nadu 620 002, India

used in filter, gas sensors etc., [14]. Nowadays, bulk as well as nano materials have potential applications in the field of optoelectronics [15]. In general the organic crystal have better NLO coefficient, but not easily obtainable and normally in a small size. Polymers can be easily fictionalized with active molecules and processed in different shapes, but they have less NLO coefficient and less stability. The catalyzed of copper in polymers and the addition of auxiliary donors is used in electro optic devices based on the NLO properties was synthesized [16, 17].

In the present investigation, we have grown UPN single crystal by slow evaporation technique and have reported structural, thermal, dielectric and optical characterization in detail.

2 Materials and methods

2.1 Crystal growth

The analytical grade of *para*-nitrophenol and urea were taken in stoichiometric ratio and dissolved in distilled water. The resultant solution was completely stirred to obtain a homogeneous solution after which it was filtered and transferred to crystal growth vessels and crystallization was allowed to take place by slow evaporation solution growth technique at room temperature. Supersaturated solution was prepared in the known amount of methanol and kept at room temperature for controlled evaporation. The yellow color single crystal of urea *para*-nitrophenol (UPN) was obtained 4 weeks with the dimensions of $11 \times 7 \times 4$ mm^3 and the photograph of the as grown crystal is shown in Fig. 2. The purity of the synthesized salt was further increased by successive recrystallization process. The reaction method of the title compound is shown Fig. 1.

2.2 Characterization

The single crystal data of the UPN compound was carried out using Bruker Kappa Apex II X-ray diffractometer with MoK$_\alpha$ radiation ($\lambda = 0.7071$ Å). The crystalline
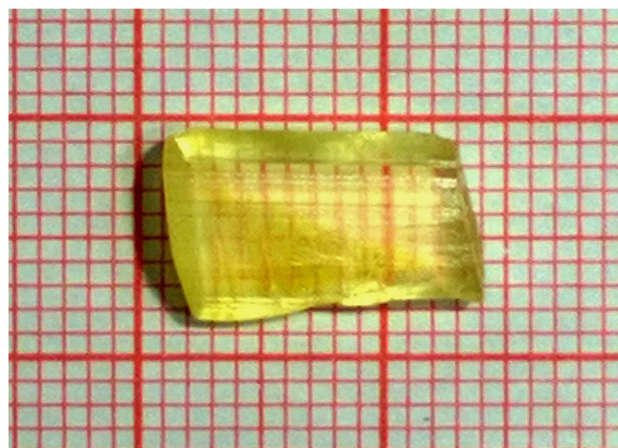
Fig. 2 As grown single crystal of UPN

perfection of the grown single crystal was checked by taking the X-ray diffraction pattern of powder samples with CuK$_\alpha$ ($\lambda = 1.5403$ Å) radiation. The elemental analysis was performed in a Perkin Elmer 2400 CHN instrument using cysteine as standard. FT-IR spectrum of UPN was recorded in the Wavenumber 400–4000 cm^{-1} using Perkin-Elmer RX1 spectrometer at 25 °C following the KBr-pellet technique. Optical absorption spectrum of UPN crystal has been recorded in the wavelength between 200 and 1100 nm using a lambda-35, UV–Vis-NIR spectrophotometer. The thermo gravimetric (TG) and differential thermal analysis (DTA) are studied using a Perkin Elmer STA 6000 system in the temperature from 15 to 900 °C at a heating rate of 10 °C/min in nitrogen atmosphere. Dielectric measurements on UPN crystal was carried out using a HIOKI 3532-50 LCR meter as a function of frequency between range 5 Hz–5 MHz and temperature 40 and 100 °C. Two opposite flat faces of the crystal were coated with conductive silver paint to act as a capacitor with the crystal acting as the dielectric medium. The electrical conductivity has been carried out using a Versa TAT impedance analyzer in the frequency range of 1 Hz–1 MHz. The second harmonic generation (SHG) efficiency of UPN was measured by a Kurtz and Perry powder technique using a Q-switched Nd:YAG laser ($\lambda = 1064$ nm). The third-order NLO properties
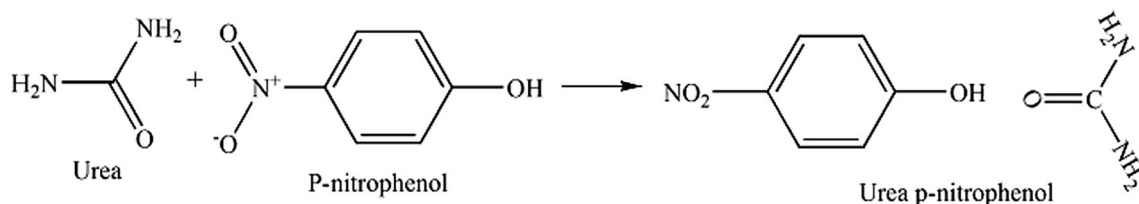
Fig. 1 Chemical reaction of UPN crystal

Table 1 Elemental analysis of UPN

UPN	N %	C %	H %	O %
Experimental	21.60	42.05	5.42	30.93
Theoretical	21.10	42.21	4.52	32.16

were estimated by Z-scan technique using the He–Ne laser source (632.8 nm) with the sample thickness 2 mm.

3 Results and discussion

3.1 Elemental analysis

The stoichiometric proportion of the constituent elements in UPN was established by elemental analysis. The experimental and calculated percentages of carbon, nitrogen, hydrogen and oxygen present in the compound are given in the Table 1. The microanalysis (CHN) of the synthesized UPN brings about a satisfactory agreement with the calculated values. This observation illustrates formation of the proposed UPN crystal.

3.2 Structural analyses

The single crystal X-ray diffraction study was carried out to confirm the cell parameters of UPN crystal. Figures 3 and 4 show the crystal packing and ORTEP structure of *para*-nitrophenol urea molecule with an atom numbering scheme. *Para*-nitrophenol molecules are linked to urea molecules by O–H…O and N–H…O hydrogen bonds,
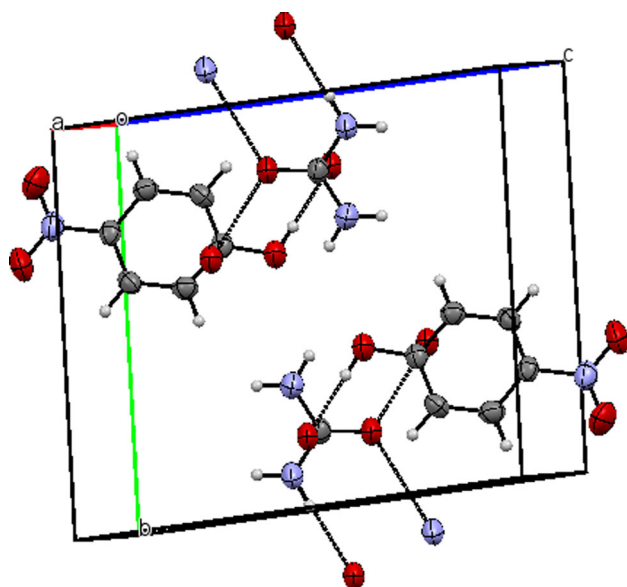
**Fig. 3** Crystal packing diagram of UPN crystal

forming a network structure [9]. The crystalline nature of the grown crystal was checked by taking the X-ray diffraction pattern of powder samples with CuK_α ($\lambda = 1.5403$ Å) radiation. The sample was scanned 2θ in the range of 10°–60° at the rate of 2°/min. The indexed powder XRD pattern is shown is Fig. 5. The appearance of sharp and strong primary peaks confirms the good crystallinity nature of the sample. The diffraction pattern contains various reflections corresponding to various crystallographic planes. As shown in Fig. 5 the peak corresponding to 2θ value 41° (1 0 2), 44° (1 1 2), 46° (2 2 0) and 55° (3 1 1) confirms the crystalline nature of the urea and 12° (0 1 1), 14° (1 0 0), 32° (0 1 4), 34° (0 3 2) and 39° (0 5 5) confirms the position of *para*-nitrophenol. It is good agreement with JCPDS card number 08-0822 and 50-2237 respectively. The estimated cell parameters are a = 3.759(2) Å, b = 10.218(4) Å, c = 11.788(8) Å, α = 98.97(7)°, β = 92.16(6)°, γ = 99.44(6)°, volume = 440.2(6) Å^3 and it belongs to triclinic system with the space group P1. The unit cell parameters are in good agreement with the reported values [9].

3.3 Vibrational studies

Vibrational analysis of the UPN crystal was elucidated from FT-IR spectrum analysis and the FT-IR spectrum is presented in Fig. 6. Aromatic nitro compounds have strong absorptions due to the asymmetric and symmetric stretching vibrations of the NO_2 group at 1570–1485 and 1370–1320 cm^{-1} respectively. The two strong peaks observed at 1487 and 1337 cm^{-1} are attributed to the N=O asymmetric and symmetric stretching vibration respectively. The scissoring mode of N=O vibrations often give rise to only IR bands in the region 800–890 cm^{-1} whereas the wagging mode shows a strong absorption in the region 700–760 cm^{-1}. These are observed in the spectrum with broad peaks at 863 and 752 cm^{-1} [18, 19].

The aromatic C–H stretching vibrations of benzene ring appear at 3111 cm^{-1} and the peak at 3390 cm^{-1} corresponds to NH_2 stretching, also the C–N group was revealed by the peak observed at 1584 cm^{-1}. In *para*-nitrophenol, the OH vibrations generally occurs at 3325 cm^{-1} whereas in the spectrum of *para*-nitrophenol urea, this peak is missing indicating that the free OH is linked to C=O of urea. Normally the –OH stretching occurs around 3325 cm^{-1}, here the –OH group of *para*-nitrophenol interacted with the carbonyl (–C=O) group of urea. Hence, the electron density around (–O–H) band transferred to the new interaction and hence it weakens. So, the characteristic frequency of OH does not appear around 3325 cm^{-1}. The other vibrations are similar to those of urea and *para*-nitrophenol [18, 19].
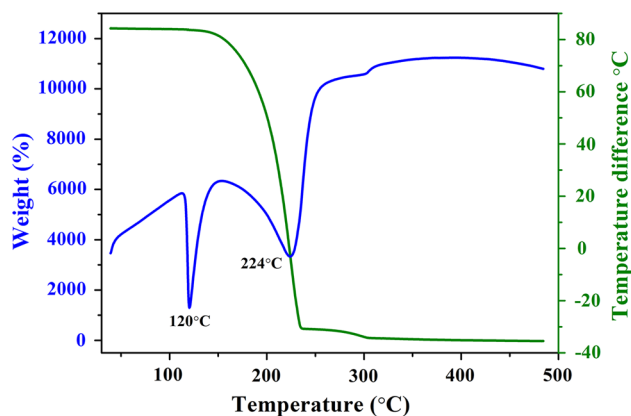
Fig. 4 ORTEP diagram of UPN molecule with atom numbering scheme
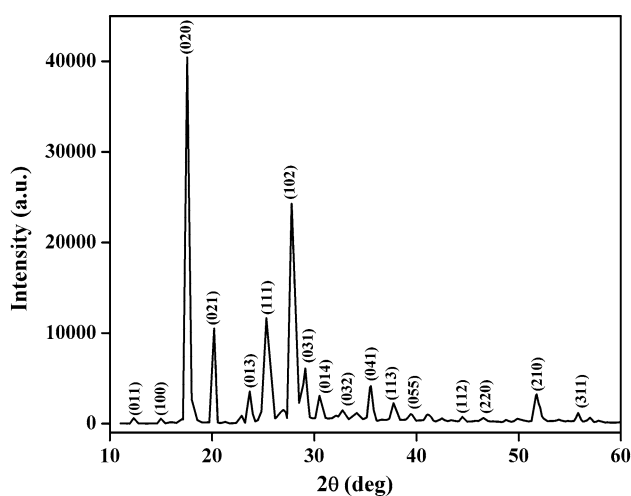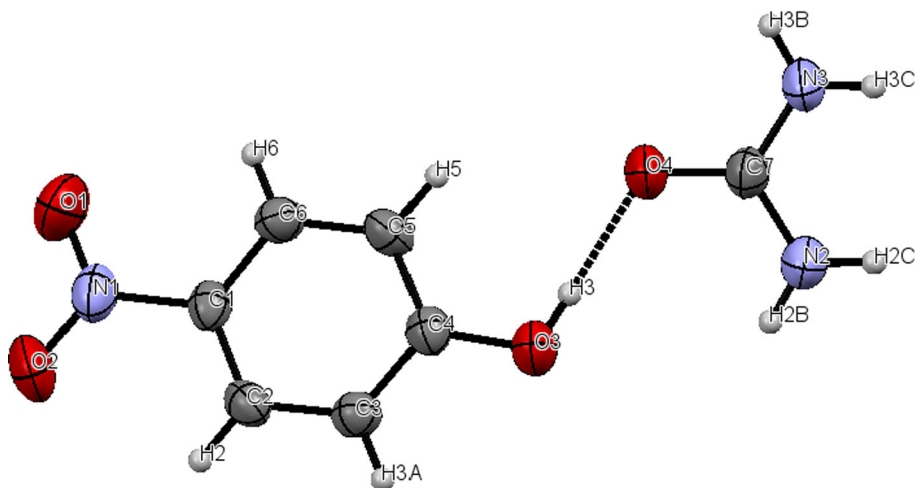
Fig. 5 Powder XRD pattern of UPN
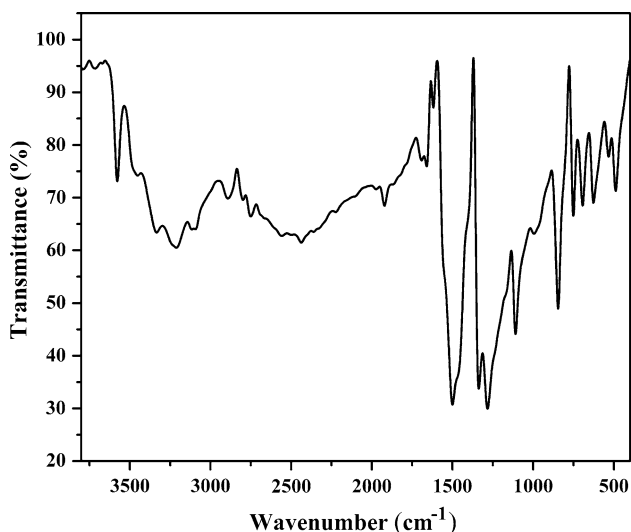
Fig. 6 FT-IR spectrum of UPN

Fig. 7 TG-DTA curve of UPN

3.4 Thermal studies

The TG–DTA curve of title crystal is shown in Fig. 7. The material is stable up to 120 °C, and then it decomposes rapidly up to 180 °C then slowly decomposes gradually 480 °C. This observation illustrates the presence of hydrated water in the crystal lattice. This is confirmed by a strong symmetric endothermic of DTA appeared at 120 °C. After liberation of crystal held water, the material gets destabilized and decomposes quickly. Hence we have a single decompose step in the TGA diagram. This second endothermic peak in DTA curve shows at 224 °C that imposes the decomposition of librated organic moiety. Hence, from thermal analysis we concluded that UPN crystal is thermally stable up to 120 °C and it is considerable material for fabrication of optoelectronic devices.
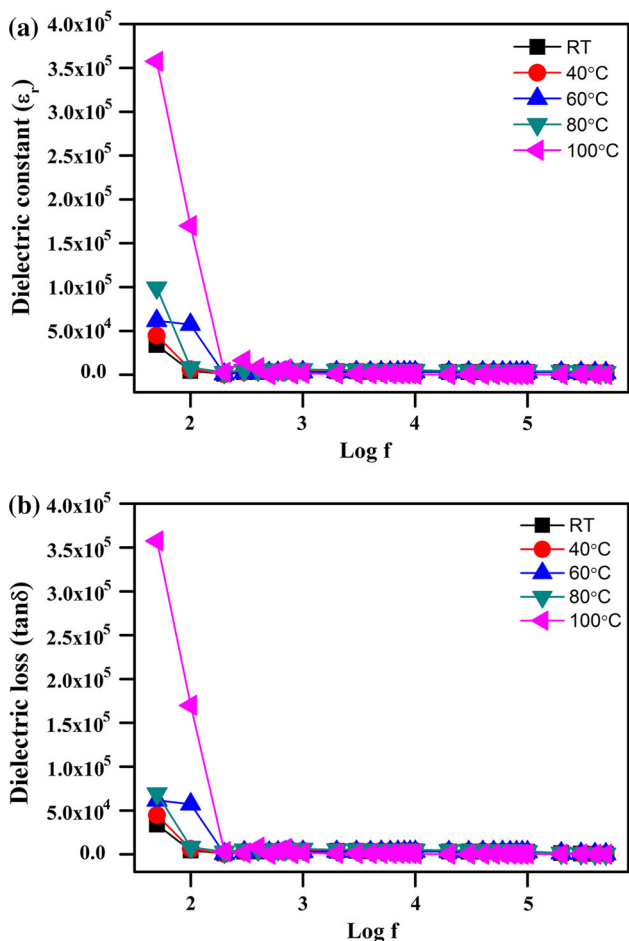
Fig. 8 **a** Frequency and temperature dependence of dielectric constant of UPN crystal. **b** Frequency and temperature dependence of dielectric loss of UPN crystal

3.5 Dielectric characterization

3.5.1 Dielectric constant and dielectric loss

Dielectric characteristics of the material are important to study to reveal the lattice dynamics of the crystal and the defects in the grown crystal [20]. The frequency and temperature response of dielectric properties of UPN crystal are as shown in Fig. 8a, b. From this figure it is observed that the dielectric constant (ε_r) decreases with increasing frequency. At low frequency all the four polarization mechanisms such as space charge, orientation, electronic and ionic are operative and hence it is found to the dielectric constant is maximum [21, 22]. As the frequency increases the dielectric constant of the material decreases, therefore these mechanisms cannot operate at the applied electric field [22].

The dielectric loss also exhibits similar behavior with increasing in frequency as shown in Fig. 8b. Decrease of

dielectric loss with the increase frequencies is attributed to oscillation of dipoles. At higher frequencies all the polarization mechanisms are not operative hence the applied energy could not sent to rotate dipoles, therefore dielectric loss decreases [23]. In addition, the dielectric constant increases with increase in temperature at low frequency. This is due the dipoles are rigidly fixed at low temperature and the applied field cannot change the condition of dipoles [24]. As the temperature increases the dipoles comparatively became free and they respond to the applied electric field. Thus the polarization increases and hence dielectric constant is also increases with increase in temperature [24]. The dielectric loss also exhibit similar behaviour with increasing temperature [21].

3.5.2 Electrical conductivity analysis

Electrical conduction in this crystal takes place as a result of electrons jumping from the low valence state to high valence state. The dc electrical conductivity at room temperature is evaluated using the relation:

$$\sigma_{dc} = \frac{d}{AR_{dc}} \tag{1}$$

where R_{dc} is the total electrical resistance of the sample. A is the cross section of the electrode, d is the thickness of the crystal. The value of R_{dc} is evaluated from the Cole–Cole plot which is drawn between real part of impedance and imaginary part of impedance as shown in Fig. 9. The dc electrical conductivity of the title crystal evaluated from the impedance spectral analysis is 4.19×10^{-8} mho/m. This low value of electrical conductivity of this crystal is due to the decrease in mobility of the charge carriers by ion
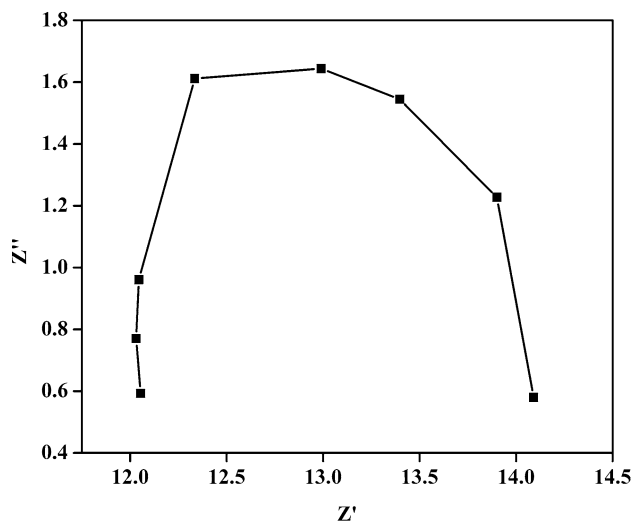
Fig. 9 Cole–Cole plot between complex impedances for UPN crystal
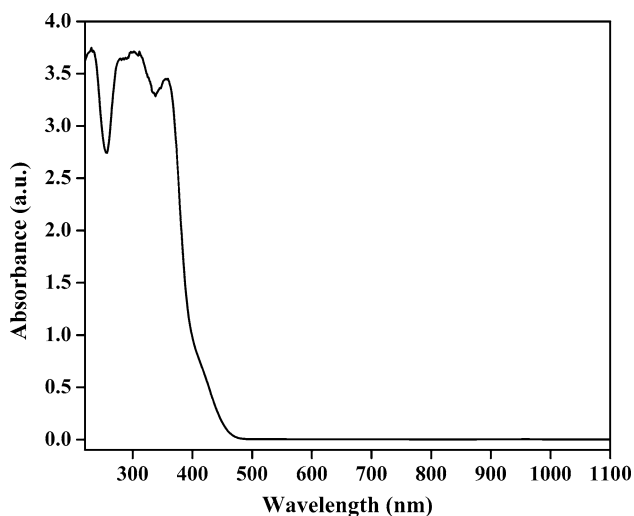
Fig. 10 The absorption spectrum of UPN

size, which brings changes in the electronic band structure [25].

3.6 Optical studies

The absorption spectrum of UPN crystal is as shown in Fig. 10. The material posses low absorption in the entire visible region. The cut-off wavelength was observed at 258 nm. It confirms the good transmission property of the title crystal in the entire visible region. The long absorption in the region between 350 and 1100 nm shows that the crystal is useful for the second-harmonic generation of Nd:YAG laser of wavelength $\lambda = 1064$ nm, which is the most desirable property of the crystal used for NLO applications. The dependence of optical absorption coefficient with the photon energy helps us to study the band
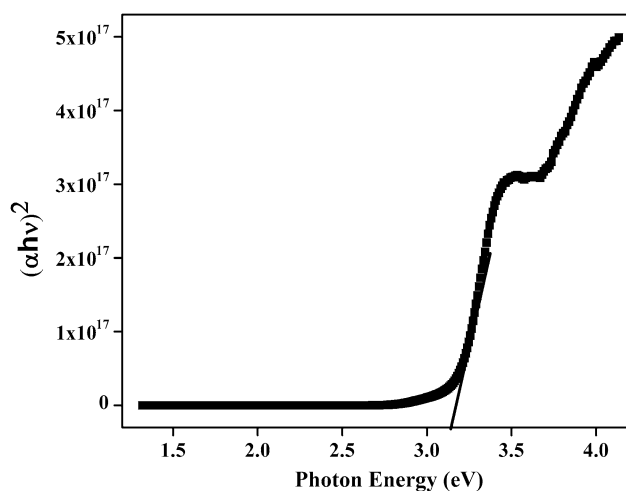
structure and the type of transition of electrons. In the photon energy region, the energy dependence of absorption coefficient suggests the occurrence of direct band gap of the crystal obeying the following equation for high photon energies (hν) [26].

$$(\alpha h\nu)^2 = A(h\nu - E_g) \qquad (2)$$

where α is the absorption coefficient, A is a constant, h is the Plank's constant, ν is the frequency of the incident beam and E_g is the optical band gap of the crystal. The variation of $(\alpha h\nu)^2$ vs photon energy (eV) is plotted in Fig. 11. The band gap of the crystal was evaluated by extrapolation of the linear part of the graph and found to be 3.18 eV. The wide band gap of the UPN crystals confirms the large transmittance in the visible region.
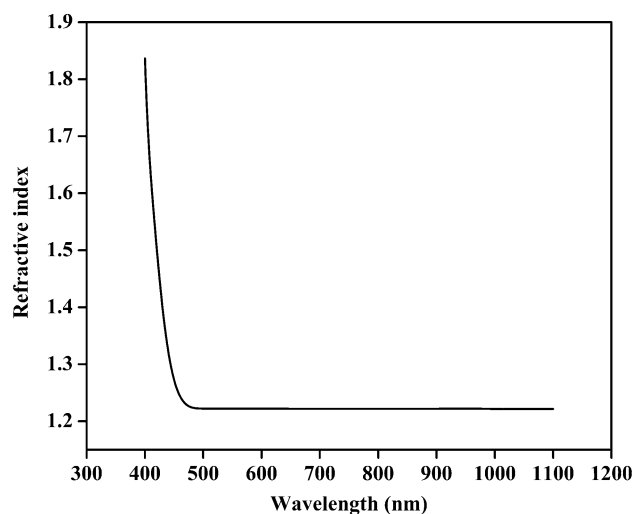
3.6.1 Refractive index extinction coefficient

When the electromagnetic wave propagates through a lossy medium, it will have some attenuation. It is owing to generation of phonons, photons, free carrier absorption and scattering [27, 28]. In such materials, refractive index becomes a complex function of frequency of the electromagnetic wave. The refractive index and extinction coefficient are calculated from the relations,
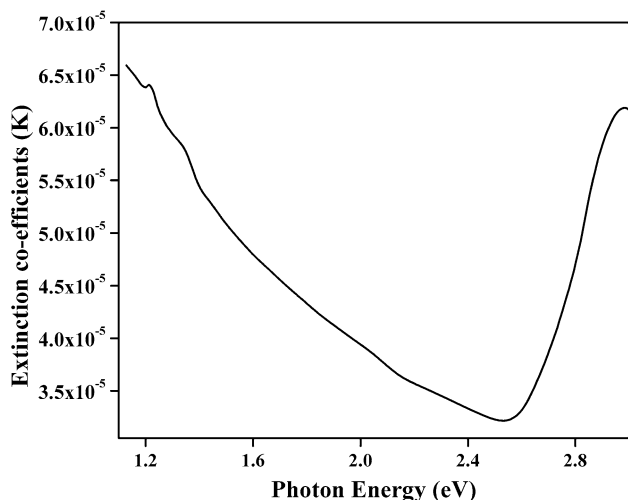
$$n = \frac{(1 + R)}{(1 - R)} - \sqrt{\frac{4R}{(1 - R)^2} - k^2}, \qquad (3)$$

$$k = \frac{\alpha\lambda}{4\pi} \qquad (4)$$

where R is the reflectance of the crystal and λ is wavelength of the incident beam. The refractive index decreases with increase of the wavelength and shown in Fig. 12.

Fig. 11 Tauc's plot of UPN

Fig. 12 Plot of wavelength versus refractive index (n)

Fig. 13 Plot of extinction coefficient versus wavelength

It is importantly noticed that the crystal has positive refractive index (n = 1.7 at 3.18 eV) with respect to energy and this indicates the focusing nature of the crystal. From the Fig. 13, it is cleared that the extinction coefficient depends on the photon energy. Since the internal energy of the device also depends on the photon energy, by tailoring the photon energy one can achieve the desired material to fabricate the optoelectronic devices.

3.7 Second harmonic generation studies

The SHG efficiency of UPN powder was determined using Kurtz and Perry powder technique [29]. In this experiment Q-switched Nd:YAG laser (1064 nm) emitting fundamental wavelength of 1064 nm was used. The grown crystal is powdered with a uniform particle size of 125–150 μm, and then packed in a microcapillary tube and exposed to the laser radiation. The SHG was confirmed by the emission of green radiation (532 nm). The input laser energy incident on the sample was 0.68 J, an energy level optimized to cause any chemical decomposition of the sample. KDP is used as a reference material for the present measurement. The SHG output efficiency of UPN is 3.8 mJ with reference to KDP 13.3 mJ.

3.8 Z-scan technique

In this method the sample is translated in the Z–direction along the axis of a focused Gaussian beam and the far field density is measured as a function of the sample positions. A spatial distribution of the temperature in the crystal surface is produced due to the localized absorption of a tightly focused beam propagating through the absorbing crystal. Hence, the spatial variation of the refractive index is

produced, which acts as a thermal lens resulting in the phase distortion of the propagating beam. The difference between peak and valley transmission (ΔT_{p-v}) is written in terms of the on-axis phase shift $|\Delta\varphi_o|$ at the focus [30, 31]. The experimental data were theoretically fitted with an equation described by Sheik-Bahae et al. [32]. The normalized transmission for the closed aperture condition is given by,

$$T(x) = 1 - \frac{4x\Delta\varphi_o}{(x^2 + 9)(x^2 + 1)} \tag{5}$$

where

$$\Delta\varphi_o = \frac{\Delta T_{p-v}}{0.406(1 - S)^{1/4}} \tag{6}$$

And the normalized transmission for the open aperture condition is

$$T(z) = (1 - q_o)/(2\sqrt{2}) \quad \text{for} \quad q_o < 1, \tag{7}$$

where,

$$q_0(z) = \frac{\beta I_0 L_{eff}}{[1 + (z/z_0)]^2} \tag{8}$$

Here β is the nonlinear absorption coefficient, I_o is the irradiance at the focus, L_{eff} is the effective length of the sample, z is the position of the sample and z_o is the Rayleigh range of the lens.

Theoretical fit of Eqs. 5 and 7 to the closed and open aperture yield values for the nonlinear refraction (n_2) and nonlinear absorption (β) (Table 2). Figure 14a shows the typical-scan data for the open-aperture setup for the solution of sample in methanol. The enhanced transmission near the focus is indicative of the saturation of absorption at high intensity [33]. Also, the absorption saturation in the sample enhances the peak and decreases the valley in the closed aperture Fig. 14b. The focusing effect is attributed to a thermal nonlinearity resulting from absorption of radiation 62.8 nm. Localized absorption of a tightly focused beam propagating through an absorbing medium produces a spatial distribution of temperature in the crystal and, consequently, a spatial variation of the refractive index that acts as a thermal lens resulting in phase distortion of the propagating beam [34] (Fig. 14a). The nonlinear absorption property of the D-π-A type π-electron system can be related closely to the π-electron conjugate degree and delocalization capacity of the molecule [35].

The typical peak—valley transmittance curve is obtained when the nonlinear refractive index of the medium is negative. The nonlinear absorption can be ascribed to saturable absorption and the nonlinear refraction leads to the self-defocusing in the crystal. The peak-valley pattern of the transmission curve obtained under the closed

**Table 2** The results of Z-scan for UPN single crystal

Material	ΔT_{p-v}	$n_2 \times 10^{-18}$ (m²/W)	$\beta \times 10^{-11}$ (m/W)	$|\chi^{(3)}| \times 10^{-12}$ (m²/W²)
UPN	1.1065	5.35	4.9994	2.8337

(a)

(b)
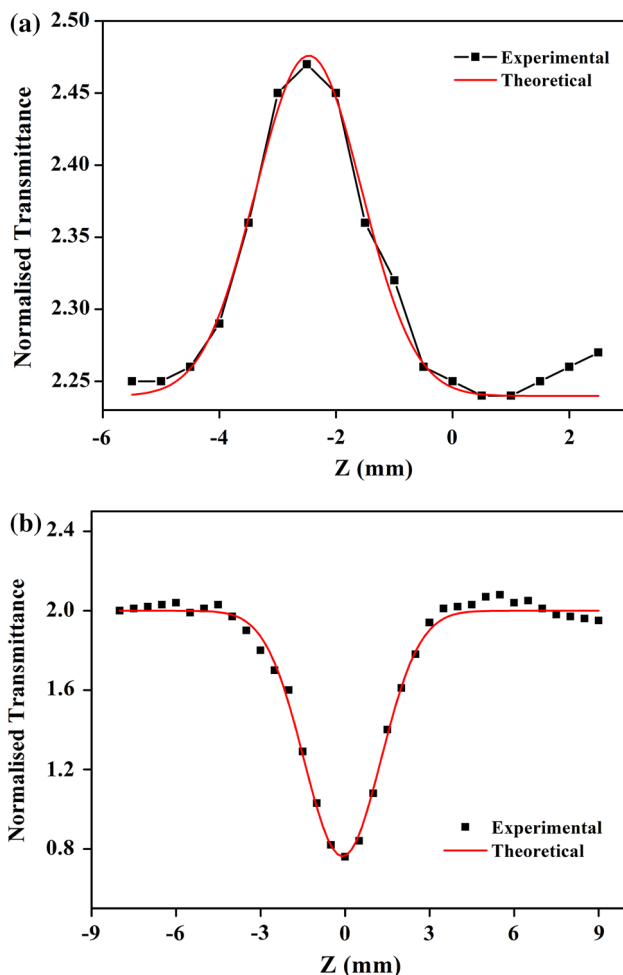
Fig. 14 **a** Normalized transmission for open aperture Z-scan. **b** Normalized transmission for closed aperture Z-scan

aperture configuration shows the characteristic self-defocusing behaviour of the propagation of the laser beam [36]. The experimentally determined values of ΔT_{P-V}, n_2, β and $|\chi^3|$ are given in Table 2.

3.9 Scanning electron microscopic analysis

The SEM analysis of as grown UNP single crystal has been performed using the instrument, Metallax-II metallurgical microscope in reflection mode. The SEM image obtained is shown in Fig. 15. It is observed from the image that the crystal has clear surface morphology except a few growth illusions, due to higher growth temperature.
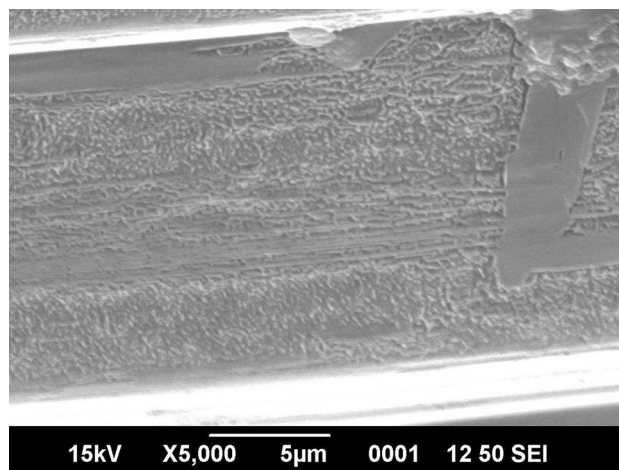
Fig. 15 SEM spectrum of UPN crystal

4 Conclusion

An organic NLO material, urea *para*-nitrophenol single crystal was grown by slow evaporation technique. The molecular structure was confirmed by the FT-IR technique and the unit-cell dimensions were determined by single crystal X-ray diffraction analysis. The optical absorption study shows that the grown crystal was optically transparent in the entire visible region with the lower cut-off wavelength of 258 nm. TG–DTA study shows that the good thermal stability of the material. Dielectric constant and loss of the crystal increase with increasing temperature. The dc electrical conductivity evaluated from the impedance spectra is found to be 4.19×10^{-8} mho/m. The SHG studies indicate that the urea *para*-nitrophenol crystals have NLO efficiency 3.5 times greater than that of standard KDP crystal. The nonlinear absorption is due to the saturable absorption while the nonlinear refraction leads to self-defocusing. The SEM photograph shows clear surface morphology except a few growth illusions on the surface. Thus, the good NLO properties, excellent optical quality makes urea *para*-nitrophenol crystals, as a potential candidate for NLO applications.

References

1. G.R. Desiraju, J. Mol. Struct. **656**, 5 (2003)

2. T.U. Devi, N. Lawrence, R.R. Babu, K. Ramamurthi, G. Bhagavannarayana, Spectrochim. Acta. A. Mol. Biomol. Specrosc. **71**, 1667 (2009)
3. S. Gowri, T. Uma Devi, D. Sajan, S.R. Bheeter, N. Lawrence, Spectrochim. Acta. A. Mol. Biomol. Spectrosc. **89**, 119 (2012)
4. K. Jagannathan, S. Kalainathan, T. Gnanasekaran, N. Vijayan, G. Bhagavannarayana, Cryst. Res. Technol. **42**, 483 (2007)
5. V. Chithambaram, S.J. Das, R.A. Nambi, S. Krishnan, Solid State Sci. **14**, 216 (2012)
6. K. Kato, IEEE J. Quantum Electron. **16**, 810 (1980)
7. D. Xue, K. Kitamura, J. Wang, Opt. Mater. (Amst). **23**, 319 (2003)
8. K.D.M. Harries, J.M. Thomas, J. Chem. Soc. Faraday Trans. **86**, 2985 (1990)
9. Y.-J. Zhao, X.-H. Li, Acta Crystallogr. Sect. E Struct. Rep. Online **61**, o3366 (2005)
10. A. Rathika, R.G. Raman, Opt. Int. J. Light Electron Opt. **125**, 2978 (2014)
11. S. Boomadevi, R. Dhanasekaran, P. Ramasamy, Cryst. Res. Technol. **37**, 159 (2002)
12. K. Sangwal, E. Mielniczek-Brzóska, J. Cryst. Growth **267**, 662 (2004)
13. J. Harrowfield, B. Skelton, A. White, Aust. J. Chem. **48**, 1333 (1995)
14. Z. Zang, M. Wen, W. Chen, Y. Zeng, Z. Xiaofeng, X. Tang, Mater. Des. **84**, 418 (2015)
15. Z. Zang, X. Tang, J. Alloys Compd. **619**, 98 (2015)
16. J. Liu, W. Gao, X. Liu, Z. Zhen, Mater. Lett. **143**, 333 (2015)
17. J. Liu, P. Si, X. Liu, Z. Zhen, Opt. Mater. **47**, 256 (2015)
18. D. Lin-Vien, N.B. Colthup, W.G. Fateley, J.G. Grasselli, *The Handbook of Infrared and Raman Characteristic Frequencies of Organic Molecules* (Academic Press, New York, 1991)
19. R.A. Nyquist, R.O. Kagel, *Infrared Spectra of Inorganic Compounds* (Academic Press, New York, 1971)
20. R.R. Babu, K. Sethuraman, N. Vijayan, G. Bhagavannarayana, Cryst. Res. Technol. **41**, 906 (2006)
21. K. Li, D. Xue, Mater. Lett. **62**, 288 (2008)
22. D. Xue, K. Kitamura, Solid State Commun. **122**, 537 (2002)
23. S. Arjunan, R. Mohan Kumar, R. Mohan, R. Jayavel, Mater. Res. Bull. **43**, 2018 (2008)
24. V. Vasudevan, R.R. Babu, G. Bhagavannarayana, K. Ramamurthi, Mater. Chem. Phys. **124**, 681 (2010)
25. J. Lee, S.M. Yoon, B. Kim, H. Lee, H.S. Song, J. Mater. Sci. **37**, 1165 (2002)
26. R. Sankar, C.M. Raghavan, M. Balaji, R.M. Kumar, R. Jayavel, Cryst. Growth Des. **7**, 348 (2007)
27. K.S. Usha, R. Sivakumar, C. Sanjeeviraja, J. Appl. Phys. **114**, 123501 (2013)
28. H.A. Bardan, M.F. Al-Mudhaffer, Q.M.A. Hassan, Y. Al-Ahmed, Chalcogenide Lett. **9**, 483 (2012)
29. S.K. Kurtz, T.T. Perry, J. Appl. Phys. **39**, 3798 (1968)
30. Q. Mohammedi Ali, P.K. Palanisamy, Opt. Int. J. Light Electron Opt. **116**, 515 (2005)
31. M. Sheik-Bahae, A.A. Said, J.H. Wei, D.J. Hagan, E.W. Vanstryland, Opt. Lett. **26**, 760 (1990)
32. M. Sheik-bahae, A.A. Said, E.W. Van Stryland, Opt. Lett. **14**, 955 (1989)
33. M. Rashidian, D. Doranian, S. Ahmadi Darani, S. Saghafi, M. Ghoranneviss, Optik **119**, 1000–1006 (2008)
34. S. Kaladevi, C. Vijayan, M.P. Kothiyal, Opt. Mater. **27**, 1606 (2004)
35. T. Cassano, R. Tommasi, M. Ferrara, F. Babudri, G.M. Farinola, F. Naso, Chem. Phys. **272**, 111 (2001)
36. L. Yang, R. Dorsinville, A. Alfano, W. Zou, N. Yang, Opt. Lett. **16**, 758 (1991)